Extracting single fiber transverse and shear moduli from off-axis misalignment fiber tensile testing

Timothy M. Harrell[1], Cole Love-Baker[1], Kenneth R. Brown[1], Clifton H. Bumgardner[1], and Xiaodong Li[1a]

[1]University of Virginia, Department of Mechanical and Aerospace Engineering, 122 Engineer's Way, Charlottesville, VA, 22904, USA
[a]xl3p@virginia.edu

Abstract

Small diameter (<100 μm) fibers (e.g. carbon fibers, Kevlar, and fiberglass) and wires (e.g. ultrafine copper and aluminum wires) are frequently used in many different engineering applications, such as for light weighting structures, electromagnetic shielding for aircraft/infrastructure/EVs, vibration damping, biological sensors, aerospace electrical devices, and electric windings just to name a few. Due to the manufacturing process, the fibers and wires are pulled and stretched to produce a preferential alignment. Therefore, thin fibers and wires typically display different properties along the length of the fiber as opposed to their cross section and many fibers/wires are considered transversely isotropic. The axial properties of fibers/wires can be ascertained via tensile testing of single-filaments or fiber tows, but the radial properties require much more effort to measure. Knowing these properties is important for the accurate prediction of micromechanical models and manipulation of fibers during micromanufacturing. In this paper, a new technique was developed to determine the transverse/shear moduli and strength of a material by conducting tensile tests of the material at increasing misalignment angles from the tensile axis. Due to the transversely isotropic nature of the material, the transverse/shear moduli and strength influence the experimental results recorded by the test machine to different degrees based on the amount of misalignment in the test setup. An equation was derived to determine the influence of each of the material properties based on the misalignment angle by

manipulating the stiffness matrix for transversely isotropic materials using the transformation matrices. Then, curve fitted coefficients were used to identify the material properties. The strengths were similarly determined by curve fitting an off-axis Tsai-Hill failure criteria to determine the influence of transverse, shear, and tensile strengths based on the complex loading condition provided by the off-axis tensile test. Zoltek Panex 35 carbon fibers were used to demonstrate this new technique and the determined properties were then compared to those obtained from nanoindentation and from literature. Fracture surfaces provide insight into the different failure mechanisms at various misalignment angles.

Keywords

Single-fiber testing; Fiber Transverse Modulus; Fiber Shear Modulus; Transverse Fiber Strength; Fiber Shear Strength; Off axis tensile testing

1 Introduction

Small diameter (< 100 μm) fibers (e.g. carbon fibers, Kevlar, and fiberglass) and wires (ultrafine copper and aluminum wires) are frequently used in many different engineering applications, such as for light-weighting structures, electromagnetic shielding for aircraft/infrastructure/EVs, vibration damping, biological sensors, aerospace electrical devices, and electric windings just to name a few. Due to the fiber manufacturing process, the fibers and wires are pulled and stretched to produce a preferential alignment. Therefore, many of these materials are considered to be transversely isotropic [1] [2] [3] [4] with the greatest modulus in the axial direction and a much lower modulus (often by an order of magnitude) in the transverse direction. Transversely isotropic materials have five independent elastic constants: the longitudinal (or axial) modulus, E_1, transverse modulus, E_2, shear modulus, G_{12}, the

major Poisson's ratio, υ_{12}, and transverse Poisson's ratio, ν_{22}. The longitudinal modulus and strength of a fiber is typically tested by manufacturers who then publish the data. The other properties, however, are often not tested because it is time consuming and require expensive specialized equipment. Studies have found the properties by using single fiber compression [5] [6], nanoindentation [1] [7] [8] [9], laser resonant ultrasound, or torsion tests [10] [11] [12]. Otherwise, they are estimated [9,13,14]. Although determining these properties may be time consuming, they are critical for accurate predictions of micromechanical models. Therefore, finding a method that can capture all these properties in one, that is less time consuming and does not require additional specialized equipment is advantageous.

Past studies of single filament tensile tests [15] [16] [17] determined that misalignment affects the measured longitudinal modulus, stress, and strain. This effect on the longitudinal modulus was generally attributed to bending. However, very thin fibers with such low dimensional stiffness that are flexible enough to be tied in knots, such as glass fibers or CFs, should be treated as a cable without bending effects [18] [19]. The results of this research [19] suggested that the effect was due to transversely isotropic material properties. Some researchers introduce misalignment in fiberglass and CF composites to estimate the shear modulus [20,21]. We extended this relationship to determine shear/transverse moduli and strengths of single filaments. Additionally, limited research has been published on the properties of the transverse and shear strength and no public data has been published on the tensile strength of a fiber in the transverse direction. Sawada and Shindo [22] measured shear strength through torsional tests. While no transverse tensile data is available, Fujita et al. [6] performed direct

transverse compressive loading on single filament fibers to determine modulus and strength properties of carbon fibers.

In this research, misalignment (off-axis) tensile testing is used to quantify transversely isotropic material properties for a single fiber. Using the linear elastic relationship and Hooke's law, an equation was developed to determine the effect of the angle of misalignment on global (experimental) tensile modulus. This global modulus involves all material properties. Shear modulus, G_{12}, and transverse modulus, E_2 have a large effect for misalignment angles greater than 30°. Single filament tensile tests were performed for varying misalignment angles between 0° and 80°. The experimental data was curve fitted to the misalignment relationship. The coefficients from the curve fitted function were used to determine the shear and tensile moduli. Similarly, the Tsai-Hill equation was used with off-axis effects to determine the effect on global strength. The strengths in the longitudinal, transverse, and shear directions (Xt, Yt, and S, respectively) were determined by curve fitting the Tsai-Hill equation.

2 Methodology

2.1 Carbon fibers

Zoltek PX35 CFs were used for this study. Zoltek's published datasheet states that the fibers have an average diameter of 7.2 μm, a tensile modulus of 242 GPa, and a tensile strength of 4.137 GPa [23]. Prior to tensile testing, the diameter of each specimen was measured optically with an Olympus BX-35 microscope.

2.2 Mechanical Testing

Single-fiber tensile tests were performed using a nanoscale tensile tester (MTS Nano Bionix UTM), which has a maximum load capacity of 500 mN and 150mm of extension. The extension of the specimen in the nanoscale tensile tester was measured by an extensometer, and the force is measured by a nanomechanical actuator (NMAT) head at the bottom grip of the specimen.

Fig. 1a shows a schematic of the experimental setup. Carbon fiber tensile samples were glued onto custom paper templates with long mount tabs, thin bridging sections are placed so that minimal load is imparted on the fiber during cutting, and triangular cutouts at the ends of the gauge section to aid in fiber placement [19]. A gauge length of 10 mm was used for all samples. The technical specifications and compliance corrections to perform the tests were in accordance with the standard ASTM C1557-14. Tensile tests were performed at a constant strain rate of 10^{-4} mm/min with a tension trigger of 750 μN. Load and displacement were recorded during the tests at a sampling rate of 10 Hz. Stress and strain were calculated. Stress-strain curves were constructed for each of the samples tested. The tensile modulus was calculated for each sample through a regression of the linear portion of the stress-strain curves. Fiber cross-sectional area was calculated for each sample using the measured diameter and used to calculate tensile strength.

Once the sample was mounted, the top grip was installed on a bidirectional linear stage to manipulate the sample in a horizontal plane. This allows for adjustment of fiber alignment relative to the tensile loading axis. The CF tensile tests were run at different angles (0°, 5°, 10°, 15°, 20°, 30°, 40°, 50°, 60°, 70°, and 80°). For each misalignment

angle, samples were tested until 10 valid tests were performed for a total of 110 data points. The angle of misalignment was measured as the angle from vertical to the centerline of the fiber (as described in [19]). The bidirectional linear stage allowed misalignment angles of up to 45°. Therefore, to conduct tests at greater misalignment angles, an extension arm (as seen in **Fig. 1b**) was manufactured. The compliance of the extension arm was deemed to be negligible by conducting zero-misalignment tests with the arm installed. No measurable compliance effect was detected. Thus, the extension arm did not require any additional compliance modification to calculate the correct stress/strain curves.

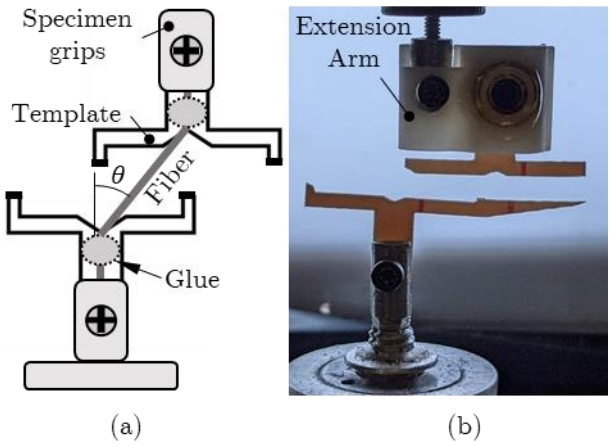

Fig. 1. (a) schematic of the experimental setup including sample, template, and grips. (b) example of 80° sample with extension arm. (Color to be used)

2.3 Imaging System

A previously developed custom stereoscopic imaging system [19] was used to measure the misalignment angle, θ, of the samples during tensile testing; see **Fig. 2**. Two FLIR BlackFly S cameras (BFS-U3-200S6M-C, 20MP, 18FPS) were mounted to a frame surrounding the tensile tester and aimed at the fibers. Image acquisition and processing was performed using a customized LabView program constructed with the

National Instrument's Vision Development Module. This setup allowed measurements of misalignment angles with an error of less than 0.1°.

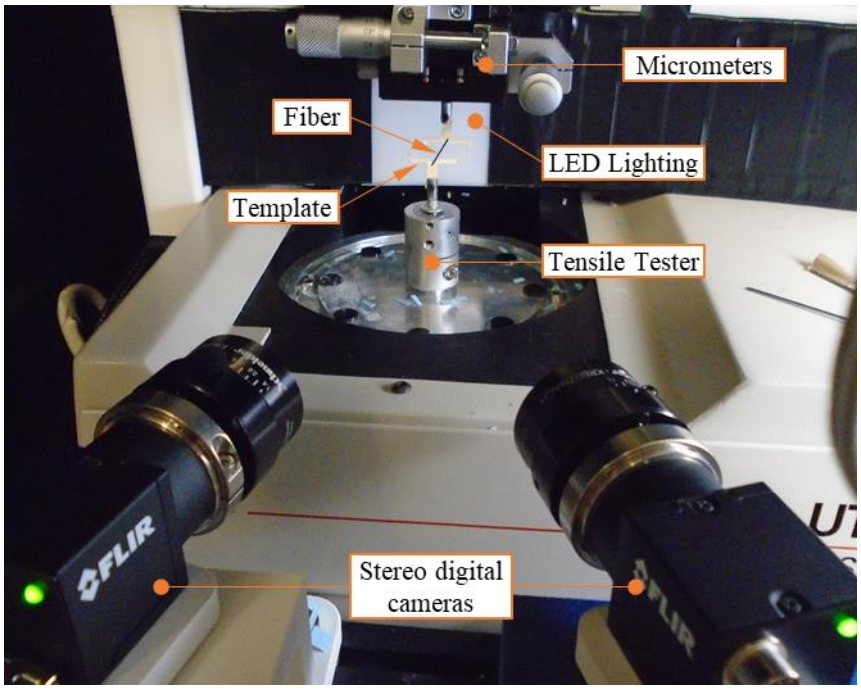

Fig. 2. Image of the camera and tensile tester setup [19] (Color to be used)

2.4 Nano-indentation

Nano-indentation tests were conducted to obtain modulus in the transverse direction. Transverse indentations were performed on the as-produced fibers encased in epoxy and polish to expose the transverse surface of the fiber. All tests were conducted on a Micro Materials Ltd. Nanotest Vantage instrument, which enabled fine displacement control with a resolution of < 0.1 nm. The indentations were performed with a diamond Berkovich indenter. An integrated optical microscope stage was used to precisely position indentations on the surface of the specimen. The elastic modulus was obtained using the Oliver-Pharr methodology [24]. 30 modulus measurements were taken along

the length of three separate fibers and averaged. The indentation depth was limited to 150 nm to account for local size effects [25] and surface curvature effects [26] [27].

3 Analytical Formulation

Fiber misalignment during tensile testing leads to off-axis loading of the fiber. To setup this problem, the fibers is mounted between two grips of the tensile machine in tension. **Fig. 3** shows a small section of the fiber with the coordinate system. The fiber is defined by the fiber coordinate system in the 1,2 direction where 1 is the longitudinal direction and 2 is the transverse direction. The tensile testing machine is defined by the global coordinate system where the origin is set at the bottom grips and vertical is the x-direction and horizontal is the y-direction. Fiber misalignment is the angle between the x-axis of the global coordinate system and the fiber's centerline, as seen defined by θ in **Fig. 3**.

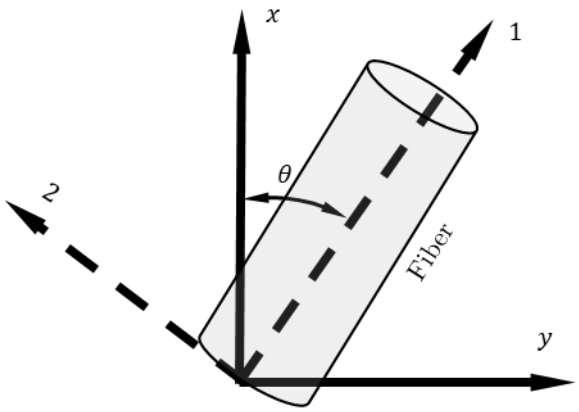

Fig. 3. CF & global coordinate systems

CF is a transversely isotropic, linear-elastic material, and is thus subject to Hooke's Law, $\sigma = E\ \varepsilon$. For a full 3-dimensional analysis, the transversely isotropic constitutive equations have six stress/strain components. To reduce the 3D problem, the fiber was not misaligned in the z-direction. This consideration reduces the problem to a 2D plane,

which results in only three remaining stress/strain components (σ_{xx}, σ_{yy}, τ_{xy}) and also reduces the five independent constants to four as the transverse Poisson's ratio, ν_{22}, is removed from stress/strain relationships. The stress-strain relationship is then as follows:

$$\begin{bmatrix} \sigma_1 \\ \sigma_2 \\ \tau_{12} \end{bmatrix} = \boldsymbol{C} \begin{bmatrix} \varepsilon_1 \\ \varepsilon_2 \\ \gamma_{12} \end{bmatrix} \tag{1}$$

where $\boldsymbol{C}$ is the stiffness matrix. The stiffness matrix is formulated using the independent material properties as follows:

$$\boldsymbol{C} = \begin{bmatrix} \dfrac{E_1}{1-\nu_{12}\nu_{21}} & \dfrac{\nu_{12}E_1}{1-\nu_{12}\nu_{21}} & 0 \\ \dfrac{\nu_{21}E_2}{1-\nu_{12}\nu_{21}} & \dfrac{E_2}{1-\nu_{12}\nu_{21}} & 0 \\ 0 & 0 & G_{12} \end{bmatrix} \tag{2}$$

The stiffness matrix is subject to the reciprocity law due to energy constraint:

$$\frac{\nu_{21}}{E_2} = \frac{\nu_{12}}{E_1} \tag{3}$$

The measured stiffness that would be determined by a direct tensile test (no misalignment) in (1) is different from that that has misalignment. To determine this a transformation must be performed. The transformation matrix that defines rotation is used in conjunction with Hooke's law to determine the stiffnesses in the global directions [28]. The transformation matrix is given by

$$[T] = \begin{bmatrix} \mathrm{c}^2 & \mathrm{s}^2 & 2\cdot\mathrm{s}\cdot\mathrm{c} \\ s^2 & \mathrm{c}^2 & -2\cdot\mathrm{s}\cdot\mathrm{c} \\ -\mathrm{s}\cdot\mathrm{c} & \mathrm{s}\cdot\mathrm{c} & c^2 - s^2 \end{bmatrix} \tag{4}$$

where $c = \cos(\theta)$ and $s = \sin(\theta)$.

Converting Hooke's law from the fiber coordinate system to the global coordinate system requires transforming both the strain and the stress in those directions. Since the cable is a 1D problem, it can only undergo strain and stress along the axis of the fiber (1-direction). Therefore, the stress and strain in the global direction are given below:

$$\begin{Bmatrix} \sigma_1 \\ \sigma_2 \\ \tau_{12} \end{Bmatrix} = [T] \begin{Bmatrix} \sigma_x \\ \sigma_y \\ \tau_{xy} \end{Bmatrix}; \begin{Bmatrix} \varepsilon_1 \\ \varepsilon_2 \\ \frac{1}{2}\gamma_{12} \end{Bmatrix} = [T] \begin{Bmatrix} \varepsilon_x \\ \varepsilon_y \\ \frac{1}{2}\gamma_{xy} \end{Bmatrix} \tag{5}$$

Substituting Equations (4) and (5) into Equation (1) and manipulating to solve for the global stress results in the modified Hooke's Law:

$$\begin{Bmatrix} \sigma_x \\ \sigma_y \\ \tau_{xy} \end{Bmatrix} = [T]^{-1} \boldsymbol{C} [T] \begin{Bmatrix} \varepsilon_x \\ \varepsilon_y \\ \frac{1}{2}\gamma_{xy} \end{Bmatrix} \tag{6}$$

The stress-loading relationship is:

$$\begin{Bmatrix} \sigma_x \\ \sigma_y \\ \tau_{xy} \end{Bmatrix} A = \begin{Bmatrix} N_x \\ N_y \\ N_{xy} \end{Bmatrix} \tag{7}$$

where A is the cross sectional area of the fiber and N_i are the load in the x, y, and xy directions.

The load cell measures in the global x-direction and therefore we will assume that N_x is the only non-zero value in the matrices. Therefore, the only stress component that can be determined is σ_x. Multiplication of equation (6) and the substitution in Hooke's law in the machine yields the following x-direction modulus:

$$E_x = \frac{E_1 c^4}{\varphi} + 2\left(\frac{\upsilon_{12}E_2}{\varphi} + 2G_{12}\right)c^2 s^2 + \frac{E_2 s^4}{\varphi} - \frac{\left(\left(\frac{E_2 + E_1}{\varphi} - 4G_{12}\right)s^2 c^2 + \frac{\upsilon_{12}E_2}{\varphi}\right)^2}{\frac{E_1 s^4}{\varphi} + 2\left(\frac{\upsilon_{21}E_2}{\varphi} + 2G_{12}\right)c^2 s^2 + \frac{E_2 c^4}{\varphi}} \tag{8}$$

where $\varphi = 1 - \upsilon_{12}^2 E_2^2 / E_1$.

Equation (8) can be simplified by using trigonometric identities. Expressions not associated with θ are condensed to a coefficient. The resulting equation is purely based on θ and E_x as follows:

$$E_x = \frac{\alpha(\beta c^4 - \beta c^2 + \gamma)}{\zeta c^4 - \eta c^2 + \kappa} \tag{9}$$

where α β, γ, ζ, η, and κ are curve fitting coefficients that relate to the material properties as follows:

$$\begin{gathered} \alpha = 4E_1, \\ \beta = E_1 E_2 - E_1 G_{12} - 2\left(\nu_{12} + \tfrac{1}{2}\right)E_2 G_{12}, \\ \gamma = E_1 E_2 / 4, \\ \zeta = E_1^2 + E_2 E_1 - 2\upsilon_{12} E_2 E_1 - 4G_{12} E_1 + 4E_2 G_{12} \nu_{12}^2, \\ \eta = 2E_1^2 - 2\upsilon_{12} E_2 E_1 - 4G_{12} E_1 + 4E_2 G_{12} \nu_{12}^2, \text{ and} \\ \kappa = E_1^2. \end{gathered} \tag{10}$$

The data fitting was carried out by a least squares regression method and was implemented in the commercial software Maple 2020 [29].

The desired moduli can be determined as a function of these curve fitting coefficients:

$$E_1 = \alpha/4$$

$$E_2 = 4\gamma/E_1 \tag{11}$$

$$G_{12} = \frac{E_2 E_1 - \beta}{E_1 - 2E_2\nu_{12} + E_2}$$

Equation (11) must assume a Poisson's ratio. To separate the shear modulus and Poisson's ratio a more complex analysis is required.

A sensitivity study was performed to understand the impact of misalignment angle on the individual material properties (longitudinal, transverse, and shear moduli and major Poisson's ratio). The results are presented in **Fig. 4**. The plots assumed the following values for carbon fibers: $E_1 = 1$, $E_2 = 0.1$, $G_{12} = 0.2$, and $\nu_{12} = 0.27$. These values were found from the properties of carbon fibers [7] [30] [31] which were averaged and then normalized against the longitudinal direction. To analyze the impact of the various material properties on the global tensile modulus (E_x), the individual properties (E_1, E_2, G_{12}, and υ_{12}) were varied to 150% and 50% of their original assumed values and plotted alongside the original assumed properties which was labeled reference (or 'Ref' for short). In addition, the maximum difference between the offset (150% and 50%) and reference plot is calculated at each misalignment angle and plotted in green.

Fig. 4a presents the sensitivity of E_1. The change in E_1 is evident at 0° and mostly influences the vertical shift of the misalignment equation at this position. Correspondingly, **Fig. 4a** shows that changes in the E_1 modulus property results in large changes at the 0° misalignment angle. **Fig. 4b** presents the sensitivity of E_2. Similarly shows that the effect of E_2 is most evident at the 90° and mostly influences the vertical

shift of misalignment equation at this position. **Fig. 4c** presents the sensitivity of G_{12} and shows that this property influences the slope of the misalignment equation between the 20° and 70° misalignment angles. The largest effect on G_{12} is 39% at 53°. The plot shows that G_{12} effects the slope in this region. Lastly, **Fig. 4d** shows the sensitivity of ν_{12}. The major Poisson's ratio only changes the experimental tensile modulus (E_x) by a maximum of 1.12% at 58°. Given this small change, the major Poisson's ratio of the fibers is not able to be extracted from these experiments.

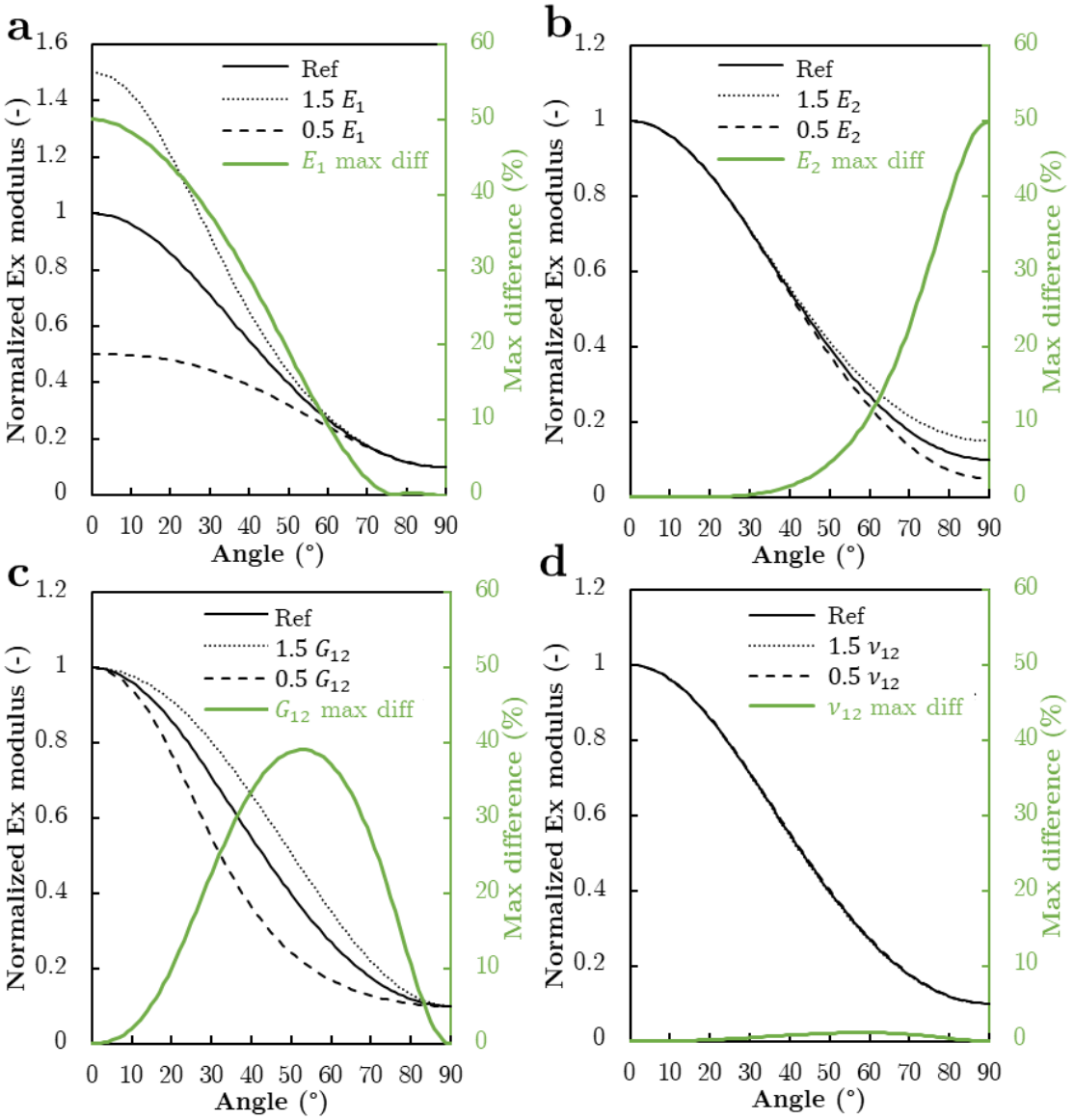

Fig. 4. Sensitivity study of misalignment results using normalized moduli for (a) E_1, (b) E_2, (c) G_{12}, and (d) ν_{12}; the green line represents the percentage difference between the reference normalized modulus and the normalized moduli when E_1, E_2, G_{12}, and ν_{12} are varied by 50% or 150%. (Color to be used)

The strength is determined using the Tsai-Hill failure criterion for a transversely isotropic material that is purely elastic [32], where:

$$\sigma_x = \sqrt{\frac{1}{\frac{c^4}{Xt^2} + \left(\frac{1}{S^2} - \frac{1}{Xt^2}\right)c^2s^2 + \frac{s^4}{Yt^2}}} \tag{12}$$

Equation (11) can be simplified using trigonometric identities. The expressions that are constant and independent of θ can be condensed into a coefficient, which allows curve fitting. The resulting equation is purely based on θ and E_x as follows:

$$\sigma_x = \sqrt{\frac{1}{\frac{c^4}{A} + Bc^2s^2 + \frac{s^4}{D}}} \tag{13}$$

where A, B, and D are curve fitting coefficients that relate to material properties as follows:

$$\begin{aligned} \mathrm{Xt} &= \sqrt{A}\,, \\ Yt &= \sqrt{D}, \text{ and} \\ S &= \frac{Xt}{\sqrt{BXt^2 + 1}} \end{aligned} \tag{14}$$

A sensitivity study was also performed to determine the influence of each strength property at different misalignment angles. The results are presented in **Fig. 5**. The plots assumed that $Xt = 1$, $Yt = 0.15$, and $S = 0.4$. **Fig. 5a** shows that X_t has a similar to E_1 with the main contribution from the 0° misalignment. **Fig. 5b** shows that Yt has the majority of its sensitivity near 90° and **Fig. 5c** shows the that S shows highest sensitivity between the 10° and 50° with the largest effect at 21°. The largest difference between the strength and modulus sensitivities is that Y_t has a high influence on the results from 30° to 90°, which will affect the results when trying to decouple the strength values. The next largest impact is the shear, S, which has a higher impact from decrease than increases, as evidenced by the difference in $1.5S$ and $0.5S$

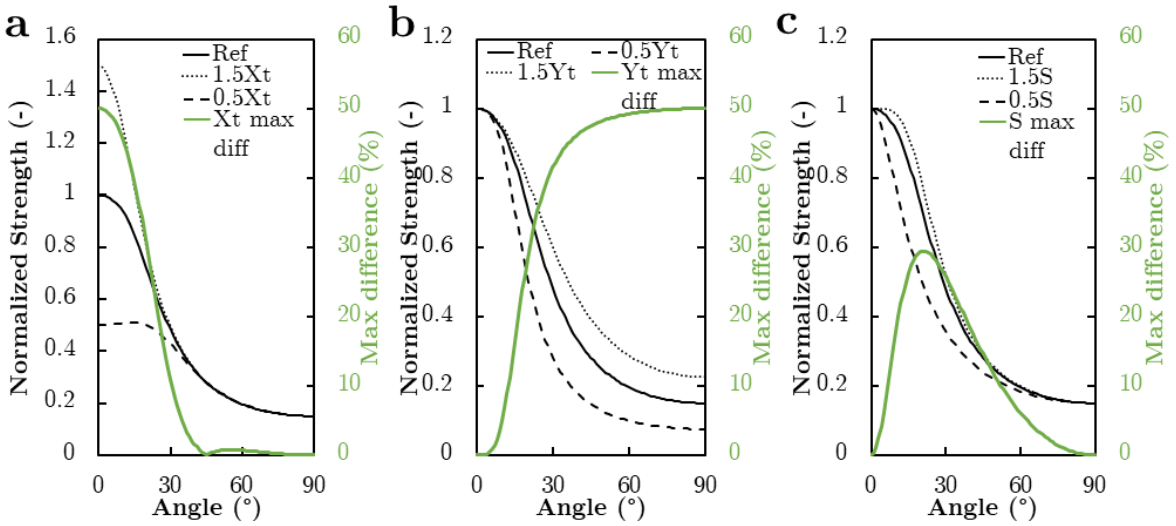

Fig. 5. Strength sensitivity study of misalignment results using normalized strengths for (a) X_t, (b) Y_t, and (c) S; the green line represents the percentage difference between the reference normalized modulus and the varied results by 50% or 150%. (Color to be used)

4 Results & Discussion

All the tensile tests exhibited linear elastic behavior up until fracture of the fibers. Upon fracture and at misalignment angles less than 60°, the fibers shatter and the resultant shock wave dislodges the fibers at the glue points until the full fiber is no longer attached to the template. Higher misalignment angles (>60°) fractures at or near the middle of the gauge length, which resulted in large fiber fragments still attached to the templates after testing. **Fig. 6** shows typical stress-strain curves for the misalignment angles examined. The figure shows that at higher misalignment angles, both the slope (or modulus) and the stress/strain to failure decrease.

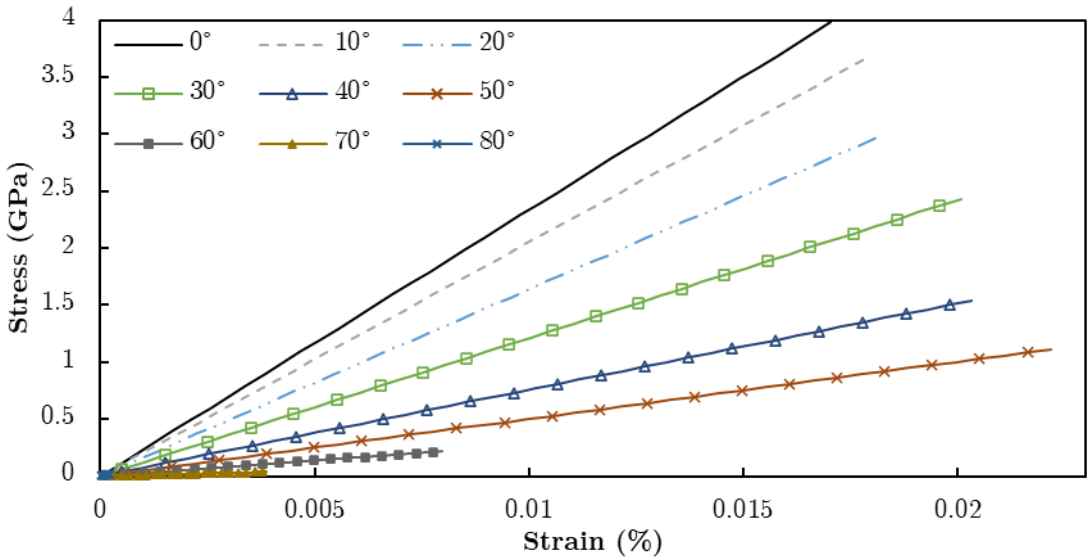

Fig. 6. Typical stress-strain curves for 0°, 10°, 20°, 30°, 40°, 50°, 60°, 70°, and 80° misalignment testing (Color to be used)

Table 1 shows the global averages of the modulus, strength, and strain at break results from different misalignment angles. CV is coefficient of variation, which is the standard deviation divided by the mean. As the misalignment angle increased, the measured modulus (global x-direction) decreased. Although the strength and strain at break also decreased with increasing misalignment angle, both the strength and strain properties showed significantly more scatter than the modulus. This is to be expected, as both strength and strain at break are strongly dependent on defects in the material [16] [33] [34].

Table 1. Experimentally determined mechanical properties of CF at all the misalignment angles

Offset angle (°)	Modulus (GPa) [CV (%)]	Strength (GPa) [CV (%)]	Strain (mm/mm) [CV (%)]
0	233.5 [13.9]	3.98 [27.8]	0.0148 [25.6]
5	211.3 [9.08]	4.07 [25.5]	0.0168 [24.7]
10	205.1 [14.5]	3.69 [29.6]	0.0154 [26.5]
15	200.5 [11.2]	4.09 [28.2]	0.0178 [29.3]
20	163.9 [11.7]	3.34 [26.7]	0.0175 [29.1]

30	121 [15.7]	2.43 [38.6]	0.0166 [42.4]
40	75.8 [22.3]	1.54 [62.8]	0.0087 [67.2]
50	50.42 [32.5]	1.11 [87.3]	0.0094 [38.9]
60	27.45 [39.5]	0.218 [93.2]	0.0034 [89.1]
70	9.684 [45.4]	0.037 [94.1]	0.00167 [92.6]
80	9.730 [52.7]	0.023 [95.6]	0.0010 [92.8]

Table 2 shows the results of the material properties derived from the experimental values using Equation (11). The longitudinal modulus and strength are slightly lower than datasheet properties, which is attributed to that single fiber tensile test is prone to small errors due to variations in the fiber. Other values are within the ranges found in literature.

Table 2. Material properties derived from misalignment test

Properties	**Values (GPa)**	**Reference Values (GPa)**	**Ref**
E_1	233	242	[23]
E_2	11.65	3.3-27.5	[1,7,8,35,36]
G_{12}	19.68	5-26	[7,22]
Xt	3.98	4.137	[23]
Yt	0.543	-	-
S	2.82	0.6-1.4	[22]

Fig. 7a shows the tensile modulus of the experimental data compared to the theoretical data. The five experimental results show good correlation. The curve fitted results determined the other properties. The nano-indentation results were very close to the measured E_2. **Fig. 7b** shows the stress at break results for the different misalignment angles. The results correlate well up to 30° and afterwards the experimental results are much lower than the theoretical predictions. This is attributed to different failure modes influencing the strength results after 30° which was examined by fractured surfaces.

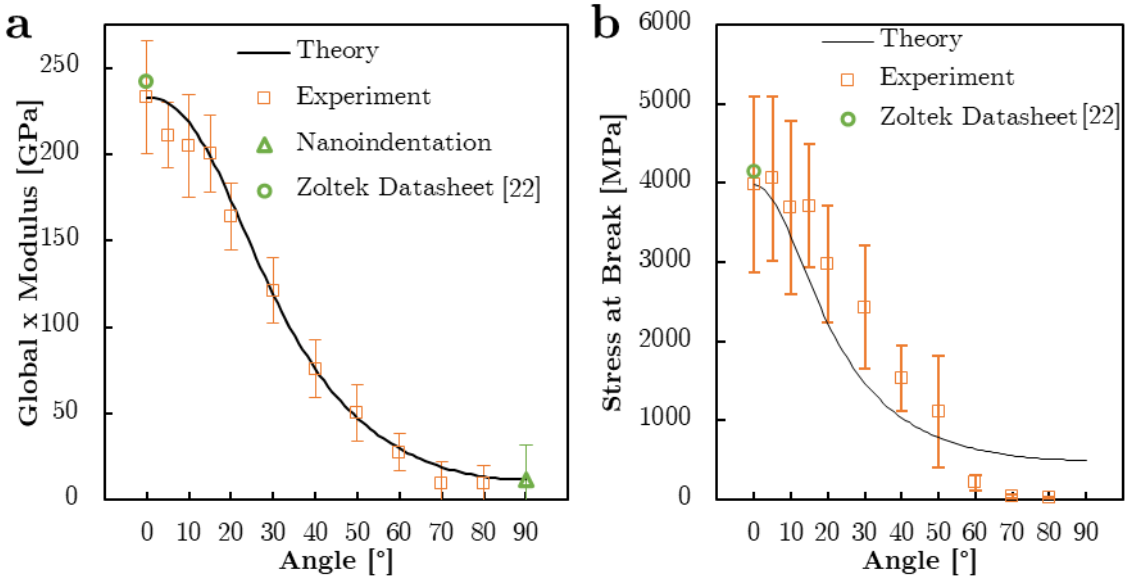

Fig. 7. Results of the curve fitting to the experimental results (Color to be used)

Fig. 8 presents SEM images of four different angles of misalignment angles (0°, 20°, 50°, and 70°). Large differences in failure are shown between the different misalignment angles. All misalignment angles show a granular surface, which is commonly observed for CF and indicates brittle tensile failure [5] [37]. Wrinkling was seen in many of the fracture surfaces of the fibers, and these wrinkles show directional characteristics that indicate a fracture initiation point. All initiation points of the fracture pattern start at the surface of the fiber and the fracture travels across the fiber. These fracture patterns show clear differences for each misalignment angle. In the 0° fracture surface, shown in **Fig. 8a**, the wrinkle propagates in all directions from the fracture initiation point. However, the fractured surfaces from higher misalignment angles (**Fig. 8b-d**) show a directional wrinkle more akin to a wave that propagates through the fiber. Upon close examination of the fracture patterns (**Fig. 8b-d**) at increasing misalignment angles, it is evident that there are two competing failure modes occurring in the fibers: shear failure and tensile failure. The granular fracture pattern is indicative of tensile failure and the wave-like fracture pattern is shear failure, as indicated in **Fig. 8b-d**.

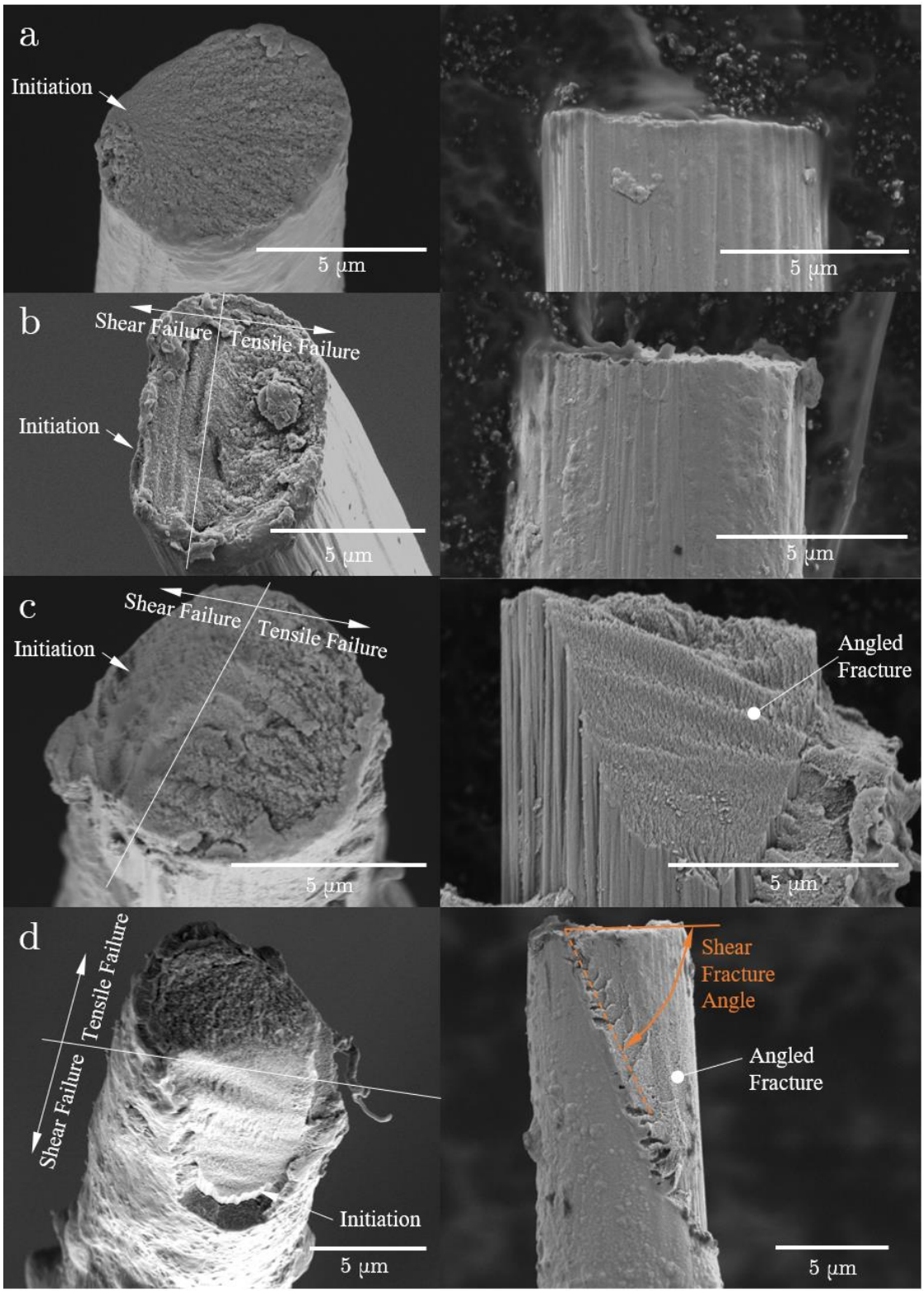

Fig. 8. SEM images of fracture surfaces of the cross section (left) and longitudinal (right) for (a) 0°, (b) 20°, (c) 50°, and (d) 70° misalignment tensile test (Color to be used)

The SEM images were used to measure shear angled fracture (exampled in **Fig. 8d)** and the different areas that failed in tension and shear. The results are shown in **Fig. 9**. The higher misalignment angles tend to produce a steeper angled shear failure segment than the lower misalignment angles. This different failure type indicates that the failure mechanism for more highly misaligned fibers starts as shear removing cross-sectional area to the fiber until the tension drives the remaining failure in a net section type failure mechanism. As the misalignment angle increased, the cross-sectional area of the fiber that failed in shear stayed constant relative to the total cross-sectional area of the fiber. The cross-sectional area of the shear failure region was approximately half (0.5 +/- 0.05) of the total fiber cross-sectional area for misalignment angles. This step-behavior is interesting to note, as it implies that there is a point where the additional misalignment does not increase the shear failure region. These results require further studies to understand the damage mechanisms caused by the misalignment.

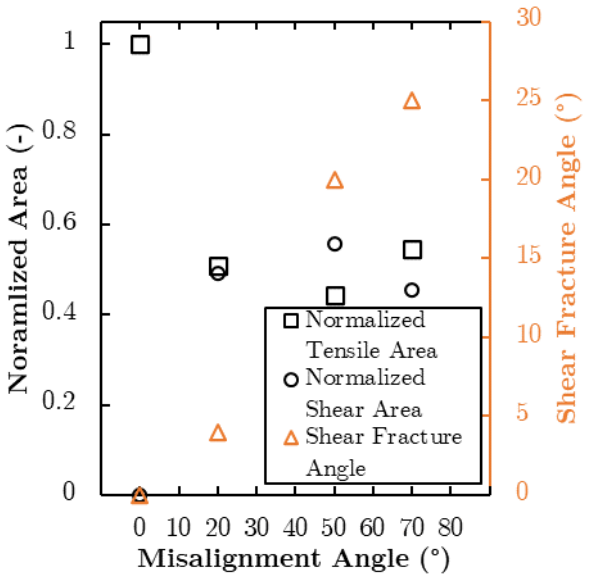

Fig. 9. Normalized tensile and shear area at different misalignment angle and shear fracture angle at different misalignment angle (Color to be used)

An additional sensitivity study was performed to determine the number of different misalignment angles needed to determine consistent transverse and shear moduli. Therefore, the E_1 modulus and Xt strength were set at the values at no misalignment and the rest of the results varied. **Table 3** presents the results of this sensitivity study. The number of misalignment angles decreased from eleven to three. Three is the minimum number of points needed for the curve fitting of all three parameters. The moduli values showed that reducing the number of data points to five had no significant difference in the results up to the fourth significant digit. This suggests that to get accurate moduli properties only 5 misalignment angles are needed. However, the strength values are more sensitive. The strength values varied significantly when reducing the number of angles. At 5 misalignment angles, the shear strength values increase significantly. This indicates that the shear strength is very susceptible to experimental data and can cause extremely high values to be produced when curve fitting. Therefore, during curve fitting, it would be worthwhile to place upper and lower limits on the shear strength. For example, the shear strength of single fibers has been experimentally found to between 20 and 70% of Xt for pitch-based and PAN-based carbon fibers [22]. Subsequently, it is suggested to carefully inspect the shear strength value.

Table 3. Sensitivity of the transversely isotropic material properties based on number of data points

Angles (°) included	**Number of angles**	E_1 **(GPa)**	E_2 **(GPa)**	G_{12} **(GPa)**	Xt **(GPa)**	Yt **(GPa)**	S **(GPa)**
0,5,10,15,20,30,40,50, 60,70,80	11	233	11.65	19.68	3.98	0.543	2.82
0, 10, 20, 30, 40, 50, 60, 70, 80	9	233	11.65	19.68	3.98	0.546	2.58
0,20,40,60,80	5	233	11.65	19.86	3.98	0.449	244
0,40,80	3	233	7.73	16.6	3.98	0.543	491

Although this paper only explored CF material, the proposed method has applicability to other fibrous and metal materials, such as other polymers (polyethylenes, nylons, etc.) or metal wires (copper, aluminum). The small size of these fibers makes it difficult to find the transverse and shear properties of a single filament. The model is limited in that ν_{12} cannot be found due to sensitivity and ν_{22} cannot be found due to the misalignment being fixed in the global xy plane. If the sensitivity can be overcome, then ν_{22} could be reintroduced by measuring 3D misalignment angles.

As noted above, shear strength is susceptible to overestimations based on experimental strength data. This is based on the complex nature of failure in the fibers and the coupling of the strength-based properties in the Tsai-Hill criteria (see **Fig. 5**).

5 Conclusions

In the present work, an experimental method was developed to determine the modulus and strength properties of a brittle transversely isotropic material: longitudinal modulus, E_1, transverse modulus, E_2, shear modulus, G_{12}, longitudinal strength, Xt, transverse strength, Yt, and shear strength, S. In this approach, misalignment between the tensile axis and the fiber axis was introduced to allow for the effects from the shear and transverse moduli/strength to be introduced into the experimental data. A formula was developed to determine the relationship between the material properties and misalignment angle. This formula was used to curve fit the experimental data and extract the material properties.

In addition, fractured surface SEM images provide insight into the different failure methods at various misalignment angles. These fractured surfaces showed that at

misalignment angles greater than 30°, there is a combined shear and net tension failure mode.

The ability to accurately determine material properties has a large impact on producing accurate predictions of micromechanical models. The practical approach shown here will allow for easier determination of the material properties for transversely isotropic materials. This method can be extended to more anisotropic materials (>5 independent constants) such as orthotropic or fully anisotropic. However, additional tests in different misalignment directions would be required to determine the additional independent constants.

6 Acknowledgment

This study was made possible through support from the U.S. Department of Energy, Office of Energy Efficiency and Renewable Energy, Vehicle Technologies Office, Award Number DE-EE0008195, and Hydrogen and Fuel Cell Technologies Office, Award Number DE-EE0009239. The authors would like to thank Zoltek for providing all of the carbon fiber samples used in this study. The authors also thank the Nanoscale Materials Characterization Facility at the University of Virginia for providing access to the SEM.

7 References

[1] T. Csanádi, D. Németh, C. Zhang, J. Dusza, Nanoindentation derived elastic constants of carbon fibres and their nanostructural based predictions, Carbon N. Y. 119 (2017) 314–325. https://doi.org/10.1016/j.carbon.2017.04.048.

[2] R.M. Christensen, Properties of carbon fibers, J. Mech. Phys. Solids. 42 (1994) 681–695. https://doi.org/10.1016/0022-5096(94)90058-2.

[3] Z. Hu, R. Karki, Prediction of mechanical properties of three-dimensional fabric composites reinforced by transversely isotropic carbon fibers, J. Compos. Mater. 49 (2015) 1513–1524. https://doi.org/10.1177/0021998314535960.

[4] R.D. Kriz, W.W. Stinchcomb, Elastic moduli of transversely isotropic graphite fibers and their composites, Exp. Mech. 19 (1979) 41–49. https://doi.org/10.1007/bf02324524.

[5] K. Naito, Y. Tanaka, J.M. Yang, Y. Kagawa, Tensile and flexural properties of single carbon fibres, ICCM Int. Conf. Compos. Mater. (2009).

[6] K. Fujita, Y. Sawada, Y. Nakanishi, Effect of Cross-Sectional Textures on Transverse

Compressive Properties of Pitch-Based Carbon Fibers, J. Soc. Mater. Sci. Japan. 50 (2001) 116–121. https://doi.org/10.2472/jsms.50.6Appendix_116.
[7] S. Duan, F. Liu, T. Pettersson, C. Creighton, L.E. Asp, Determination of transverse and shear moduli of single carbon fibres, Carbon N. Y. 158 (2020) 772–782. https://doi.org/10.1016/j.carbon.2019.11.054.
[8] R. Maurin, P. Davies, N. Baral, C. Baley, Transverse properties of carbon fibres by nano-indentation and micro-mechanics, Appl. Compos. Mater. 15 (2008) 61–73. https://doi.org/10.1007/s10443-008-9057-3.
[9] H. Miyagawa, T. Mase, C. Sato, E. Drown, L.T. Drzal, K. Ikegami, Comparison of experimental and theoretical transverse elastic modulus of carbon fibers, Carbon N. Y. 44 (2006) 2002–2008. https://doi.org/10.1016/j.carbon.2006.01.026.
[10] C.L. Tsai, I.M. Daniel, Determination of shear modulus of single fibers, Exp. Mech. 39 (1999) 284–286. https://doi.org/10.1007/BF02329806.
[11] M. Ishikawa, Y. Kogo, J. Koyanagi, F. Tanaka, T. Okabe, Torsional modulus and internal friction of polyacrylonitrile- and pitch-based carbon fibers, J. Mater. Sci. 50 (2015) 7018–7025. https://doi.org/10.1007/s10853-015-9254-z.
[12] H. Behlow, D. Saini, L. Oliveira, L. Durham, J. Simpson, S.M. Serkiz, M.J. Skove, A.M. Rao, Direct measurement of shear properties of microfibers, Rev. Sci. Instrum. 85 (2014). https://doi.org/10.1063/1.4895679.
[13] J.C. Halpin, Effects of Environmental Factors on Composite Materials, Wright-Patterson Air Force Base, Ohio 45433, 1969.
[14] T. Mori, K. Tanaka, Average stress in matrix and average elastic energy of materials with misfitting inclusions, Acta Metall. 21 (1973) 571–574. https://doi.org/10.1016/0001-6160(73)90064-3.
[15] X. Li, X. Wang, W.C. Chang, Y.J. Chao, M. Chang, Effect of tensile offset angles on micro/nanoscale tensile testing, Rev. Sci. Instrum. 76 (2005). https://doi.org/10.1063/1.1865732.
[16] F. Islam, S. Joannès, S. Bucknell, Y. Leray, A. Bunsell, L. Laiarinandrasana, Investigation of tensile strength and dimensional variation of T700 carbon fibres using an improved experimental setup, J. Reinf. Plast. Compos. 39 (2020) 144–162. https://doi.org/10.1177/0731684419873712.
[17] F. Islam, S. Joannès, L. Laiarinandrasana, Evaluation of Critical Parameters in Tensile Strength Measurement of Single Fibres, J. Compos. Sci. 3 (2019) 69. https://doi.org/10.3390/jcs3030069.
[18] C.T. Herakovich, Mechanics of Fibrous Composites, 1st ed., John Wiley & Sons Inc, New York, NY, 1998.
[19] C.A. Love-Baker, T.M. Harrell, K.R. Brown, C.H. Bumgardner, X. Li, Analyzing the effect of misalignment on single-filament carbon fiber tensile testing via stereoscopic computer vision imaging, Meas. Sci. Technol. 32 (2021) 065904. https://doi.org/10.1088/1361-6501/abeceb.
[20] F. Pierron, A. Vautrin, The 10° off-axis tensile test: A critical approach, Compos. Sci. Technol. 56 (1996) 483–488. https://doi.org/10.1016/0266-3538(96)00004-8.
[21] G. Odegard, M. Kumosa, Determination of shear strength of unidirectional composite materials with the Iosipescu and 10°off-axis shear tests, Compos. Sci. Technol. 60 (2000) 2917–2943. https://doi.org/10.1016/S0266-3538(00)00141-X.
[22] Y. Sawada, A. Shindo, Torsional properties of carbon fibers, Carbon N. Y. 30 (1992) 619–629. https://doi.org/10.1016/0008-6223(92)90181-U.
[23] Zoltek Technologies, Technical Datasheet ZOLTEK™ PX35, 2016. http://zoltek.com/products/panex-35/.
[24] W.C. Oliver, G.M. Pharr, An improved technique for determining hardness and elastic modulus using load and displacement sensing indentation experiments, J. Mater. Res. 7 (1992) 1564–1583. https://doi.org/10.1557/JMR.1992.1564.
[25] Z. Xu, X. Li, Sample size effect on nanoindentation of micro-/nanostructures, Acta Mater. 54 (2006) 1699–1703. https://doi.org/10.1016/j.actamat.2005.11.043.
[26] S. Miyake, E. Sasaki, T. Kato, T. Namazu, Curvature-corrected hardness measurement technique for nanoindentation of bonding wire, Sensors Mater. 28 (2016) 153–161. https://doi.org/10.18494/SAM.2016.1165.
[27] Q.P. McAllister, J.W. Gillespie, M.R. Vanlandingham, Nonlinear indentation of fibers, J. Mater. Res. 27 (2012) 197–213. https://doi.org/10.1557/jmr.2011.336.
[28] M.W. Hyer, Stress Analysis of Fiber-Reinforced Composite Materials, 1998.
[29] Maplesoft, Maplesoft 2020 User Manual, (2020).
[30] D.D.L. Chung, Carbon Fiber Composites, Butterworth-Heinemann, Newton, MA, 1994.

https://doi.org/10.1016/B978-0-08-050073-7.50010-5.
[31] I. Krucinska, T. Stypka, Direct measurement of the axial poisson's ratio of single carbon fibres, Compos. Sci. Technol. 41 (1991) 1–12. https://doi.org/10.1016/0266-3538(91)90049-U.
[32] C. Herakovich, Mechanics of Fibrous Composites, 1st ed., John Wiley & Sons Inc, New York, NY, 1997.
[33] Y. Nordström, R. Joffe, E. Sjöholm, Mechanical characterization and application of Weibull statistics to the strength of softwood lignin-based carbon fibers, J. Appl. Polym. Sci. 130 (2013) 3689–3697. https://doi.org/10.1002/app.39627.
[34] C.P. Beetz, A self-consistent Weibull analysis of carbon fibre strength distributions, Fibre Sci. Technol. 16 (1982) 81–94. https://doi.org/10.1016/0015-0568(82)90027-6.
[35] K. Naito, Y. Tanaka, J.M. Yang, Transverse compressive properties of polyacrylonitrile (PAN)-based and pitch-based single carbon fibers, Carbon N. Y. 118 (2017) 168–183. https://doi.org/10.1016/j.carbon.2017.03.031.
[36] D. Mounier, C. Poilane, C. Bucher, P. Picart, Evaluation of transverse elastic properties of fibers used in composite materials by laser resonant ultrasound spectroscopy, Proc. Acoust. 2012 Nantes Conf. (2012) 1247–1250.
[37] Y.Y. Wang, G.P. Wu, R.M. Li, X.L. Li, C.X. Lu, Fracture mechanisms of polyacrylonitrile-based high-strength type carbon fibers, Fibers Polym. 15 (2014) 2541–2543. https://doi.org/10.1007/s12221-014-2541-5.